SUPPLEMENTAL INFORMATION

A

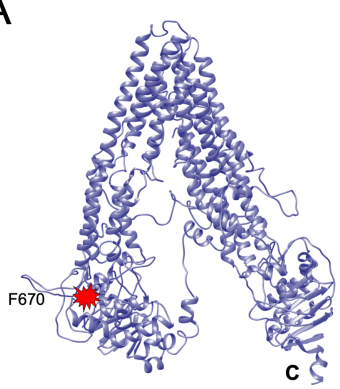

S. cerevisiae Yor1

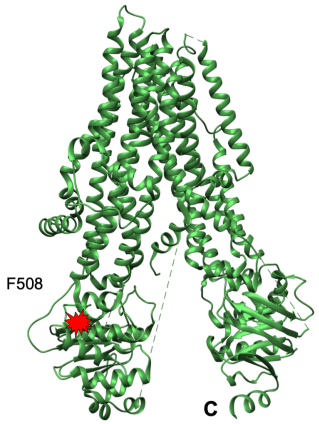

H. sapiens CFTR

B

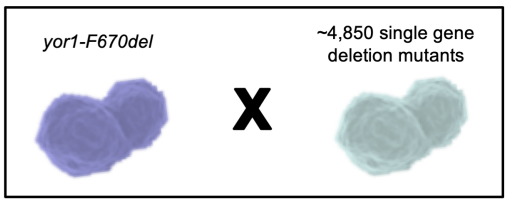

Identify increased oligomycin resistance (i.e. reduced 'ΔL' score) in corresponding haploid *yor1-F670del* / *geneKO* double mutants

Ribosome region	Yeast gene	Human gene	Eukaryotic (e) or universal (u) name	'ΔL' score
P Stalk	*RPP2*	*RPLP2(αβ)*	P2	-27.7
P Stalk + GAC	*RPL12*	*RPL12*	uL11	-28.1
GAC	*RPL9*	*RPL9*	uL6	-23.0
	RPL16	*RPL13A*	uL13	-25.6
	RPL40	*RPL40*	eL40	-18.8
PET	*RPL4*	*RPL4*	uL4	-28.2
	RPL13	*RPL13*	eL13	-20.7
	RPL35	*RPL35*	uL29	-20.0
	RPL37	*RPL37*	eL37	-23.1
	RPL39	*RPL39*	eL39	-35.6

C

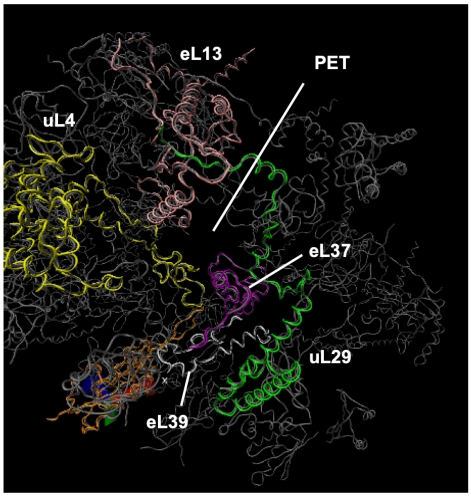

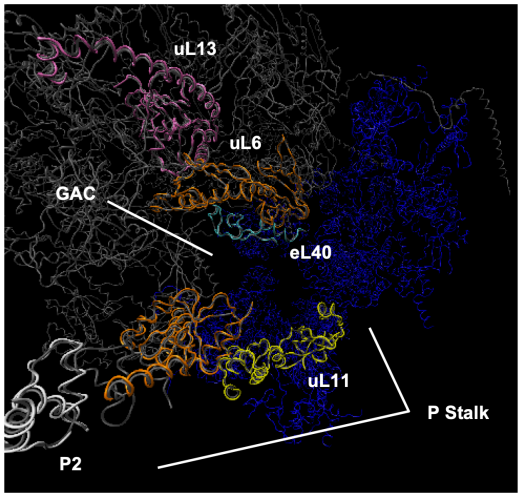

Supplemental Figure 1. Genome-wide phenomic screening in *S. cerevisiae* reveals ribosomal mediators of CFTR folding. (A) Structural comparison of Yor1 (PDB file 4F4C) (1) and CFTR (PDB file 5UAK) (2, 3), indicating position of the F670 residue (Yor1) that corresponds to F508 (CFTR). (B) In combination with Yor1-F670del, individual gene knockout (*geneKO*) mutants from the yeast deletion strain library were systematically tested for capacity to restore efflux of the mitochondrial toxin, oligomycin (4). Prominent targets included ribosomal protein L12A, otherwise annotated as RPL12/uL11 in humans (5). 'ΔL' is based on growth curve analysis and denotes the influence of gene deletion on the time required to reach half maximal carrying capacity in the presence of increasing, growth-inhibitory concentration of oligomycin (see (6, 7)). Thus, the 'ΔL' score correlates inversely with the capacity of the gene knockout to increase biogenesis of Yor1-F670del. (C) Proteins listed in panel (B) are mapped to the eukaryotic ribosome (8). Left: Hits that surround the peptide exit tunnel (PET) include uL4 (yellow), eL13 (pink), eL37 (purple), uL29 (green), and eL39 (light grey). Right: Targets residing in the GTPase-associated center (GAC) and/or P stalk are uL13 (magenta), uL6 (orange), eL40 (light blue), uL11 (yellow), and P2 (white).

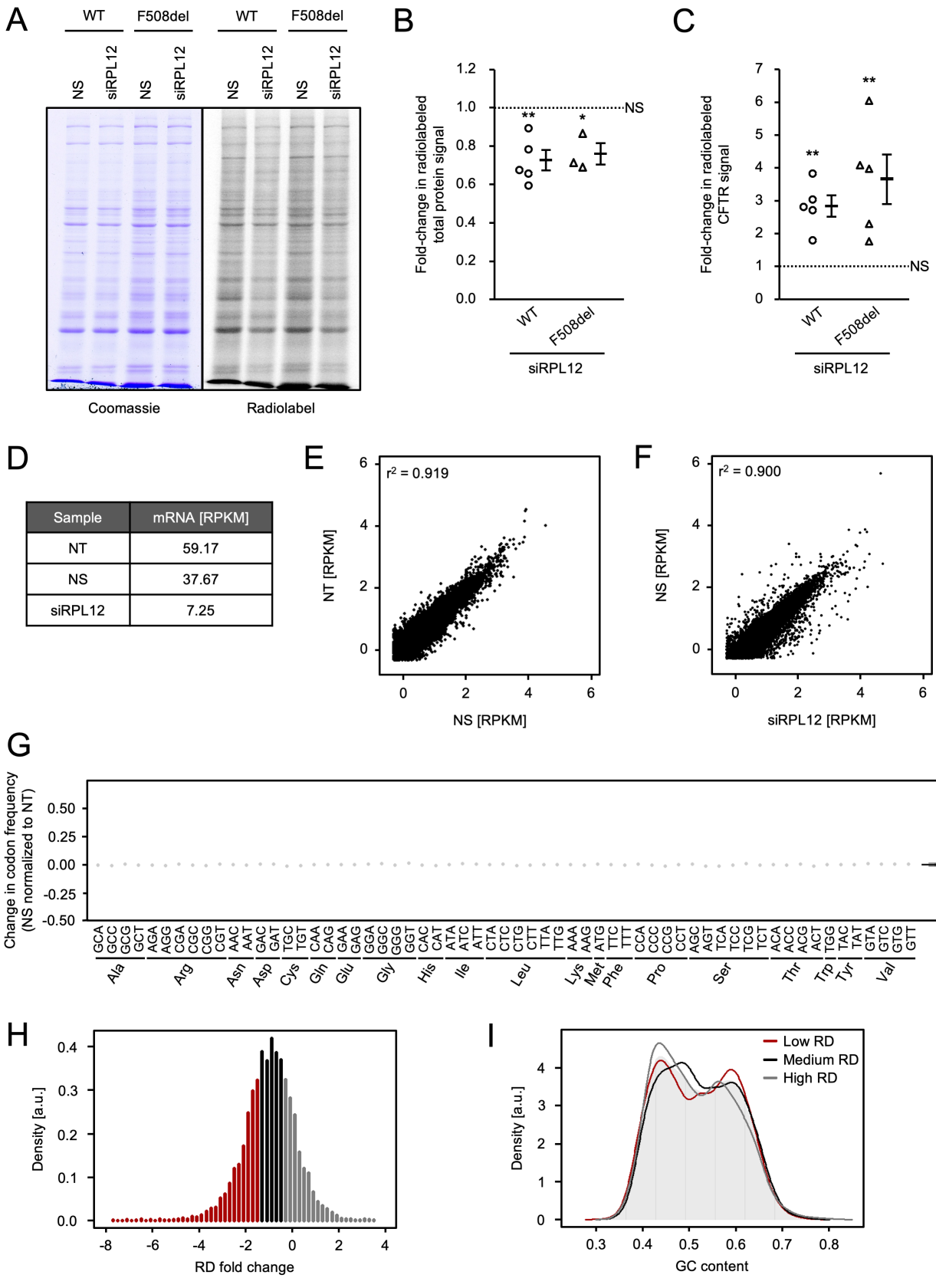
A
WT
F508del
WT
F508del
NS
siRPL12
NS
siRPL12
NS
siRPL12
NS
siRPL12
Coomassie
Radiolabel
B
Fold-change in radiolabeled total protein signal
1.2
1.0
0.8
0.6
0.4
0.2
0.0
NS
**
*
WT
F508del
siRPL12
C
Fold-change in radiolabeled CFTR signal
7
6
5
4
3
2
1
0
**
**
NS
WT
F508del
siRPL12
D
Sample
mRNA [RPKM]
NT
59.17
NS
37.67
siRPL12
7.25
E
r2 = 0.919
NT [RPKM]
NS [RPKM]
F
r2 = 0.900
NS [RPKM]
siRPL12 [RPKM]
G
Change in codon frequency (NS normalized to NT)
0.50
0.25
0.00
-0.25
-0.50
GCA GCC GCG GCT AGA AGG CGA CGC CGG CGT AAC AAT GAC GAT TGC TGT CAA CAG GAA GAG GGA GGC GGG GGT CAC CAT ATA ATC ATT CTA CTC CTG CTT TTA TTG AAA AAG ATG TTC TTT CCA CCC CCG CCT AGC AGT TCA TCC TCG TCT ACA ACC ACG ACT TGG TAC TAT GTA GTC GTG GTT
Ala Arg Asn Asp Cys Gln Glu Gly His Ile Leu Lys Met Phe Pro Ser Thr Trp Tyr Val
H
Density [a.u.]
0.4
0.3
0.2
0.1
0.0
-8 -6 -4 -2 0 2 4
RD fold change
I
Density [a.u.]
4
3
2
1
0
Low RD
Medium RD
High RD
0.3 0.4 0.5 0.6 0.7 0.8
GC content

Supplemental Figure 2. ^{35}S-incorporation and deep sequence analysis in CFBE. (A) Representative Coomassie and radiolabeled images of CFBE stably expressing WT- or F508del-CFTR, both treated with non-specific (NS) siRNA or siRNA directed against RPL12 (siRPL12). Cells were labeled for 15 minutes with ^{35}S-methionine and ^{35}S-cysteine and lysates analyzed by SDS-PAGE. (B),(C) Quantification of radioactive signals corrected for protein amount (Coomassie stain) from panel (A). RPL12 knockdown decreases total protein expression by ~20-25% (B), yet augments WT- and F508del-CFTR levels ~200-300% (C). Data include mean ± SEM obtained from siRPL12-treated cells normalized to NS controls (dotted line; set to 1) (n = 3-5). Asterisks represent statistical comparison between siRPL12 and NS siRNA. *, $p < 0.025$; **, $p < 0.01$ (unequal variance *t*-test on $\log_2$-transformed data with post-hoc Bonferroni correction; $\alpha = 0.025$). (D) RPL12 mRNA expression in non-treated (NT), NS, or siRPL12-treated cells as computed from the RNA-Seq data set. (E),(F) Application of NS (E) or RPL12 (F) siRNA did not globally alter mRNA as revealed by comparative transcriptome analysis of the RNA-Seq data set (NS, $r^2 = 0.919$; siRPL12, $r^2 = 0.900$; Pearson correlation coefficient). (G) No significant alterations in ribosome dwelling occupancy (y-axis) were detected for NS siRNA-treated CFBE as compared to NT cells. Difference in ribosome occupancy between NT and NS siRNA-treated CFBE is quantified for single codons (represented as dots) and for all codons (box-plot on right). Note that for many codons, the change in RDO was nearly zero. For additional details, see Figure 2 legend (panels D and E). (H) RPL12 silencing effects on RD, expressed as fold-change with respect to RD values obtained after siRPL12 treatment. Transcripts were divided into three equal expression categories and designated as least (red), median (black), or most (grey) abundant RD ($p = 0.008$, low vs high RD groups; $p = 0.0015$, median vs high RD groups; two-sided Kolmogorov-Smirnov test). The top functional categories (GO terms)

enriched in the intermediate gene group (black) included several pathways reflecting essential cellular functions unaffected by RPL12 siRNA, such as rRNA processing (enrichment score 5.11), regulation of mRNA stability (enrichment score 3.61), proteasome-mediated ubiquitin-dependent catabolic processes (enrichment score 3.61), NIL/NFkB signaling (enrichment score 3.61), and positive regulation of ubiquitin-protein ligase activity in the mitotic cycle (enrichment score 3.61). (I) GC content of the three designated expression groups defined in panel (H). For comparison, GC content of all expressed transcripts in CFBE41o$^-$ cells is also shown (grey shaded area). Note the characteristic asymmetry of the TA/GC content of the human transcriptome previously reported (9).

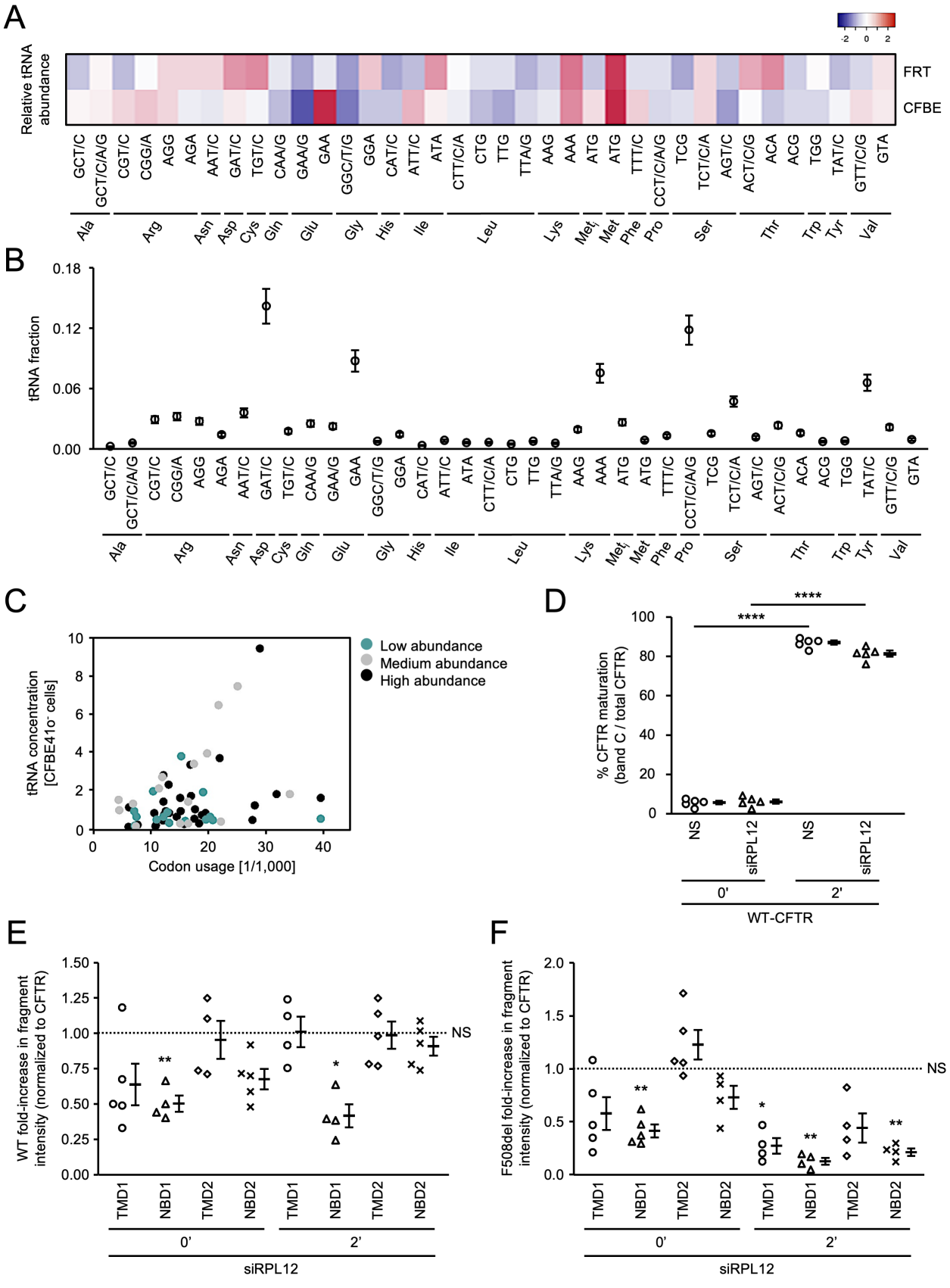
A
Relative tRNA abundance
-2
0
2
FRT
CFBE
GCT/C
GCT/C/A/G
CGT/C
CGG/A
AGG
AGA
AAT/C
GAT/C
TGT/C
CAA/G
GAA/G
GAA
GGC/T/G
GGA
CAT/C
ATT/C
ATA
CTT/C/A
CTG
TTG
TTA/G
AAG
AAA
ATG
ATG
TTT/C
CCT/C/A/G
TCG
TCT/C/A
AGT/C
ACT/C/G
ACA
ACG
TGG
TAT/C
GTT/C/G
GTA
Ala
Arg
Asn
Asp
Cys
Gln
Glu
Gly
His
Ile
Leu
Lys
Met$_i$
Met
Phe
Pro
Ser
Thr
Trp
Tyr
Val
B
tRNA fraction
0.18
0.12
0.06
0.00
C
tRNA concentration [CFBE41o- cells]
Codon usage [1/1,000]
Low abundance
Medium abundance
High abundance
D
% CFTR maturation (band C / total CFTR)
****
****
NS
siRPL12
NS
siRPL12
0'
2'
WT-CFTR
E
WT fold-increase in fragment intensity (normalized to CFTR)
NS
TMD1
NBD1
TMD2
NBD2
0'
2'
siRPL12
F
F508del fold-increase in fragment intensity (normalized to CFTR)
NS
siRPL12

Supplemental Figure 3. tRNA microarrays and CFTR proteolysis in CFBE. (A) Microarrays of tRNA abundance in CFBE and FRT epithelia are represented relative to HeLa cells (n = 3-5 repeats per condition). (B) Absolute tRNA concentrations in CFBE are presented as fractions of the total tRNA amount and determined from the comparative arrays in panel (A) using previously measured absolute tRNA concentrations in HeLa cells (10). All data presented include mean ± SEM (n = 3-5 per panel). (C) tRNA concentration in CFBE cells poorly correlates with genomic codon usage ($r^2 = 0.11$, Pearson correlation coefficient). The top 15 codons pairing to low (green), medium (grey), or high (black) abundance tRNAs are shown (n = 3-5 repeats per condition). (D) Quantification of WT-CFTR maturation (band C/total CFTR) in response to RPL12 suppression (see also Figure 5B). Data include mean ± SEM (n = 4-5). ****, $p < 0.0001$ (unequal variance *t*-test on $\log_2$-transformed data with post-hoc Bonferroni correction; $\alpha = 0.0125$). (E),(F) Fold-change of domain-specific fragment intensities for WT- (E) or F508del-CFTR (F) (see also Figure 5B). Note that NS-treated F508del signal in the 2-hour chase is less than 2-fold over background. Individual bands are quantified and corrected for total radiolabeled CFTR. Data include mean ± SEM obtained from siRPL12-treated cells normalized to NS controls (dotted line; set to 1) (n = 4-5). Asterisks represent statistical comparison between siRPL12 and NS siRNA. *, $p < 0.0125$; **, $p < 0.01$ (unequal variance *t*-test on $\log_2$-transformed data with post-hoc Bonferroni correction for each time point; $\alpha = 0.0125$).

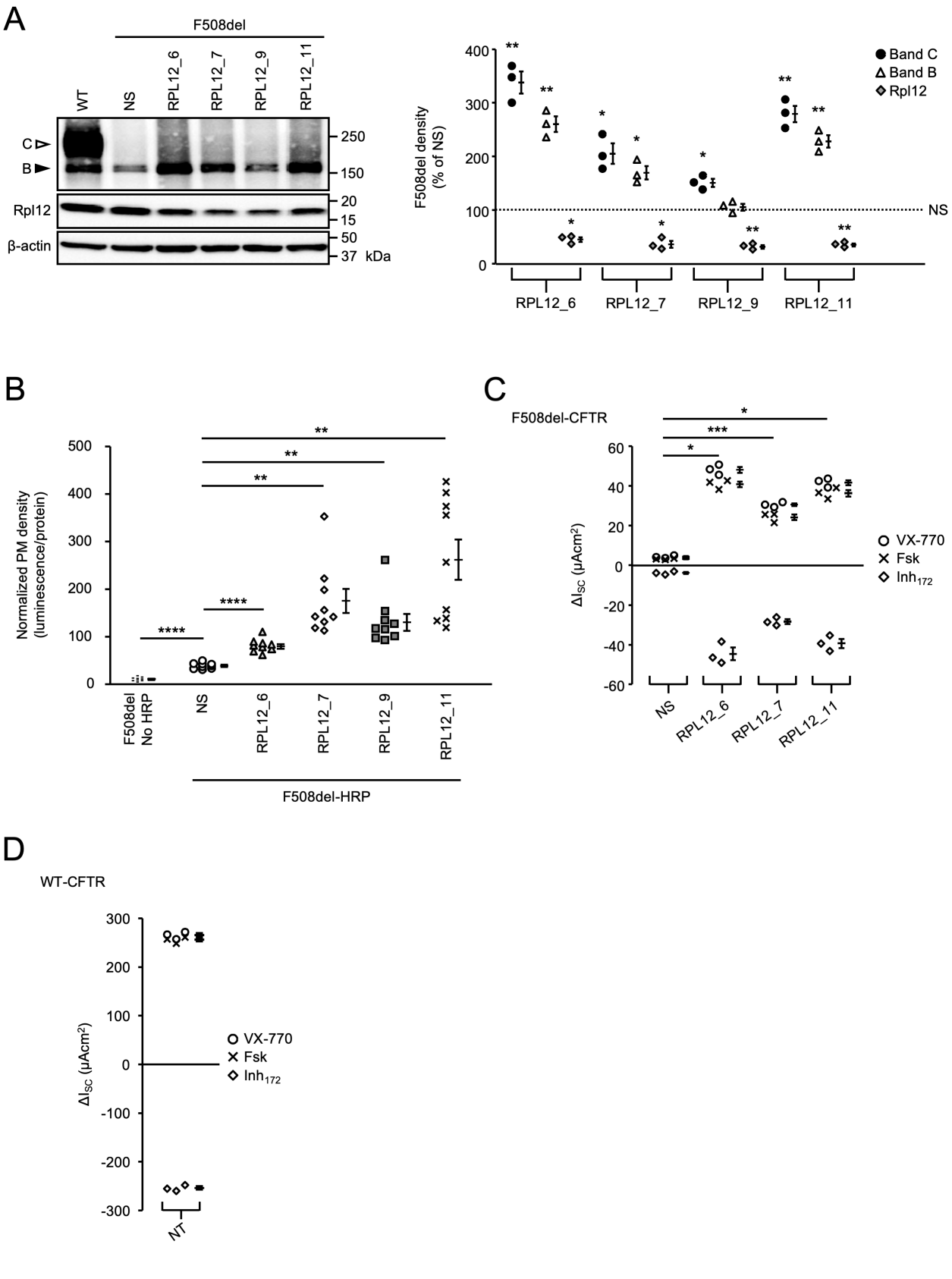
A
F508del
WT
NS
RPL12_6
RPL12_7
RPL12_9
RPL12_11
C
B
Rpl12
β-actin
250
150
20
15
50
37 kDa
F508del density (% of NS)
Band C
Band B
Rpl12
NS
RPL12_6
RPL12_7
RPL12_9
RPL12_11
B
Normalized PM density (luminescence/protein)
F508del No HRP
NS
RPL12_6
RPL12_7
RPL12_9
RPL12_11
F508del-HRP
C
F508del-CFTR
ΔISC (μAcm2)
VX-770
Fsk
Inh172
NS
RPL12_6
RPL12_7
RPL12_11
D
WT-CFTR
ΔISC (μAcm2)
VX-770
Fsk
Inh172
NT

Supplemental Figure 4. Rpl12 suppression rescues the F508del-CFTR biogenesis defect in FRT cells. (A) Expression levels of immature (band B, closed arrowhead) and mature (band C, open arrowhead) F508del-CFTR are augmented following ~50-70% reduction in Rpl12 expression. Quantification of immunoblot data are included on right. Data include mean ± SEM obtained from siRPL12-treated cells normalized to NS siRNA controls (dotted line; set to 100%) (n = 3). Asterisks represent statistical comparison between siRPL12 and NS siRNA. *, $p < 0.0167$; **, $p < 0.01$ (unequal variance *t*-test on $\log_2$-transformed data with post-hoc Bonferroni correction for each siRNA; $\alpha = 0.0167$). (B) Horseradish peroxidase (HRP)-tagged F508del-CFTR (modified extracellular loop 4) displays increased PM localization in response to knockdown by multiple siRNAs directed against Rpl12. Data include mean ± SEM (n = 9). Statistical comparisons are annotated by horizontal bars. **, $p < 0.001$; ****, $p < 0.00001$ (two-sample *t*-test with post-hoc Bonferroni correction; $\alpha = 0.00833$). (C) F508del-CFTR ion transport activity is increased using distinct Rpl12 siRNAs (100nM, 4 days) (n = 3). Asterisks represent statistical comparison of forskolin+VX-770 stimulation (i.e. total constitutive plus activated CFTR function) versus NS siRNA. *, $p < 0.0125$; ***, $p < 0.0001$ (two-sample *t*-test with post-hoc Bonferroni correction; $\alpha = 0.0125$). (D) Baseline short-circuit current measurement of WT-CFTR expressed in FRT cells. Data include mean ± SEM (n = 3). WT, wild-type; NT, non-treated; NS, non-specific siRNA; RPL12_6, _7, _9 and _11 denote RPL12 siRNAs with cross-reactivity against the rat mRNA; Fsk, forskolin (5μM); VX-770 (5μM); Inh_{172}, CFTR $Inhibitor_{172}$ (10μM).

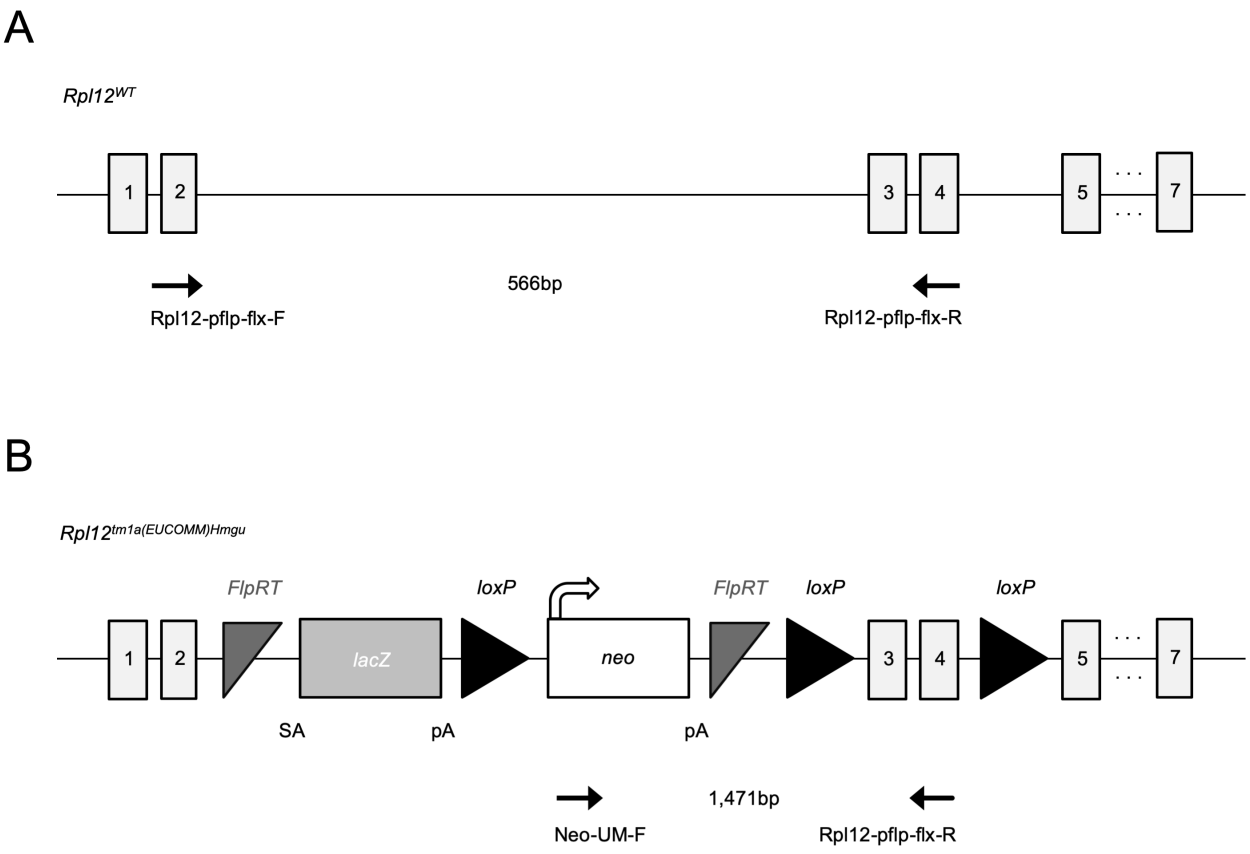

Supplemental Figure 5. Schematic of 'knockout first' construct utilized for generation of *Rpl12* heterozygous mice. (A) Wild-type *Rpl12* allele. Animals carrying this gene were labeled *Rpl12*$^{+/+}$. (B) 'Knockout first' *Rpl12*$^{tm1a(EUCOMM)Hmgu}$ allele containing *lacZ*-tagged insertion and *loxP*-flanked *neo*-driven selection cassette (Helmholtz Zentrum München, Neuherberg, Germany). Mice harboring this construct were identified as *Rpl12*$^{+/-}$. Forward (F) and reverse (R) primers are indicated for each allele with specific sequences provided in Supplemental Table 2. *FlpRT*, flippase recombinase target; *loxP*, locus of crossover in P1; *lacZ*, lactose operon gene Z encoding β-galactosidase; *neo*, neomycin; UM, universal mouse; SA, splice acceptor site; pA, poly-A sequence.

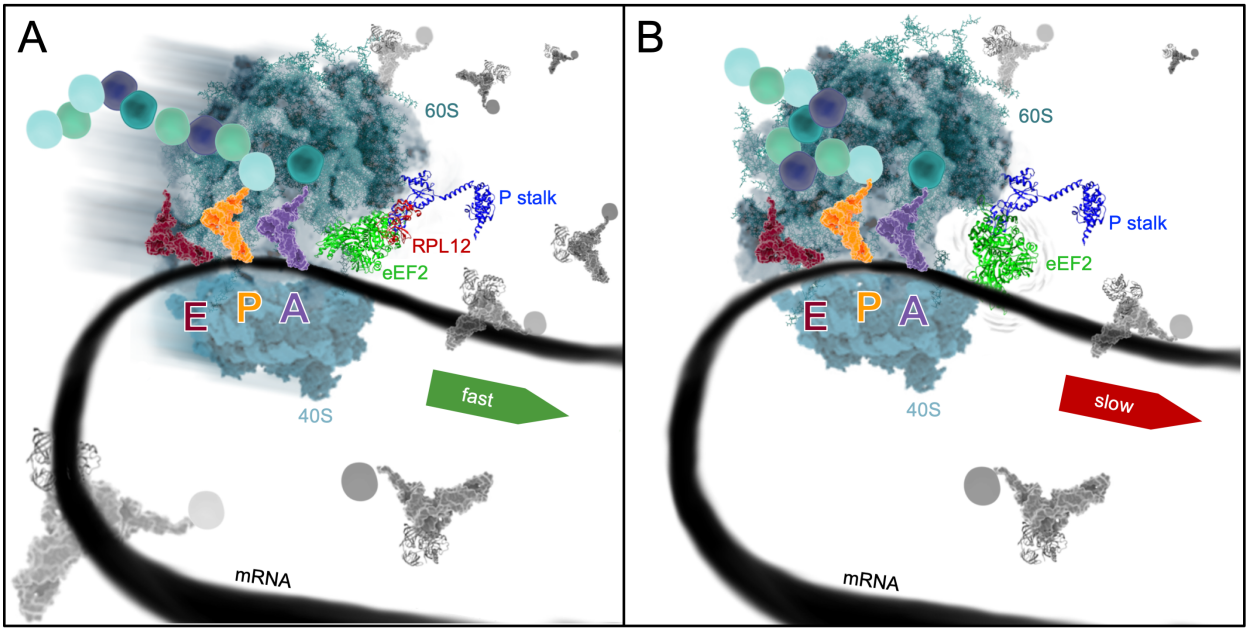

Supplemental Figure 6. Proposed mechanism of RPL12 silencing effect on translation elongation. (A) RPL12 (red), located at the base of the 60S P stalk (blue) (PDB file 4V6X) (8), resides within the GTPase-associated center and facilitates interaction with several GTP-bound translation factors, including eEF2 (green) (8, 11, 12). Under physiologic conditions, RPL12 mediates interaction of eEF2 with aminoacylated (aa)-tRNAs in the A-site (violet). Following transpeptidation, eEF2 hydrolyzes GTP to translocate aa-tRNA from the A- to P-site (orange), which facilitates translation of mRNA (black) at an average rate of 5-6 codons per second (13). (B) When RPL12 is depleted, eEF2 is not able to bind efficiently to the GTPase-associated center, and the process of peptidyl-tRNA translocation is slowed. As a result, ribosome velocity is reduced (see Figure 2). For visualization purposes, decoding by the ribosome is represented in cross-section.

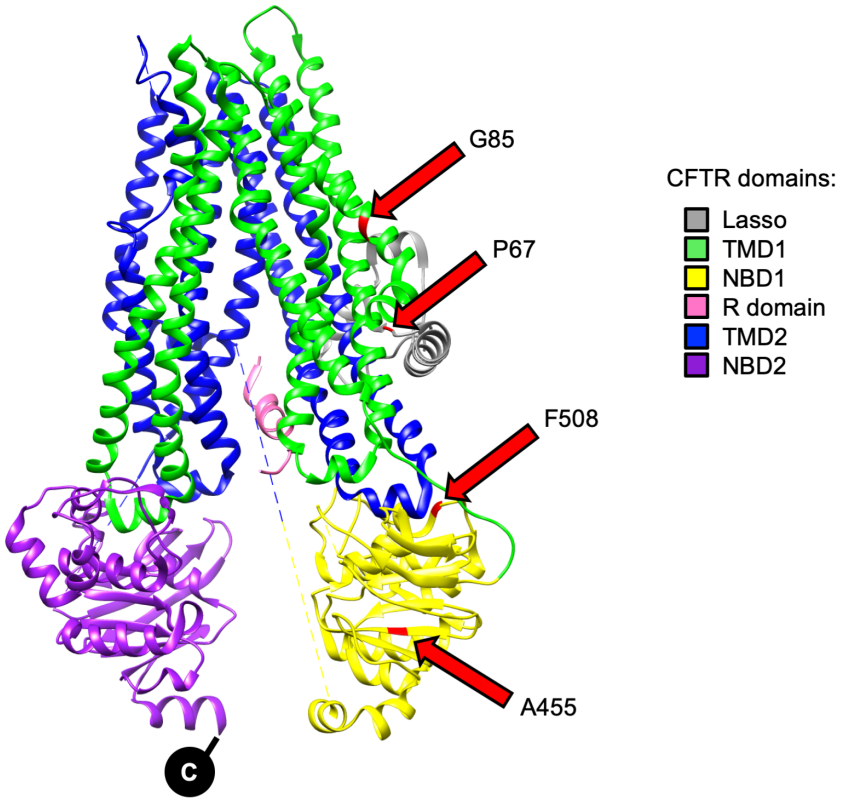

Supplemental Figure 7. Structural annotation of CFTR variants investigated in this study. P67L is located just downstream of lasso helix 2 (grey), whereas G85E resides in TMD1 (green). F508del and A455E localized to NBD1 (yellow). CFTR structure was formatted using PDB file 5UAK (2, 3).

Supplemental Table 1. siRNAs used in this study.

Gene Symbol	Product Name	Target Sequence
RPL12	Hs_RPL12_6	5' – CAGCCAGTTAAGCACAAAGGA – 3'
RPL12	Hs_RPL12_7	5' – CCCAACGAGATCAAAGTCGTA – 3'
RPL12	Hs_RPL12_9	5' – CCTGATCATCAAAGCCCTCAA – 3'
RPL12	Hs_RPL12_11	5' – AACCACCAAGAGACAGAAAGA – 3'
Non-specific (NS)	Negative Control	5' – AATTCTCCGAACGTGTCACGT – 3'

Supplemental Table 2. PCR primers used for *Rpl12* mouse line validation.

Allele	Primer ID	Orientation	Target Sequence	PCR Product Size
$Rpl12^{WT}$	Rpl12-pflp-flx-F	Forward	5'-TGGCCTGTAGATGTGTTCTGTC-3'	566 bp
	Rpl12-pflp-flx-R	Reverse	5'-GATTCCTGAGGGCTGCTATCTC-3'	
$Rpl12^{tm1a(EUCOMM)Hmgu}$	Neo-UM-F	Forward	5'-AGGATCTCCTGTCATCTCACCTTGCTCCTG -3'	1471 bp
	Rpl12-pflp-flx-R	Reverse	5'-GATTCCTGAGGGCTGCTATCTC-3'	

REFERENCES

1. Jin MS, et al. Crystal structure of the multidrug transporter P-glycoprotein from Caenorhabditis elegans. *Nature.* 2012;490(7421):566-569.

2. Liu F, et al. Molecular structure of the human CFTR ion channel. *Cell.* 2017;169(1):85-95.

3. Zhang Z, Chen J. Atomic structure of the cystic fibrosis transmembrane conductance regulator. *Cell.* 2016;167(6):1586-1597.

4. Louie RJ, et al. A yeast phenomic model for the gene interaction network modulating CFTR-ΔF508 protein biogenesis. *Genome Med.* 2012;4(12):103.

5. Ban N, et al. A new system for naming ribosomal proteins. *Curr Opin Struct Biol.* 2014;24:165-169.

6. Hartman JL IV, et al. Yeast phenomics: An experimental approach for modeling gene interaction networks that buffer disease. *Genes.* 2015;6(1):24-45.

7. Veit G, et al. Ribosomal stalk protein silencing partially corrects the ΔF508-CFTR functional expression defect. *PLoS Biol.* 2016;14(5):e1002462.

8. Anger AM, et al. Structures of the human and Drosophila 80S ribosome. *Nature.* 2013;497(7447):80-85.

9. Touchon M, et al. Transcription-coupled TA and GC strand asymmetries in the human genome. *FEBS Lett.* 2003;555(3):579-582.

10. Kirchner S, et al. Alteration of protein function by a silent polymorphism linked to tRNA abundance. *PLoS Biol.* 2017;15(5):e2000779.

11. Ito K, et al. Molecular insights into the interaction of the ribosomal stalk protein with elongation factor 1α. *Nucleic Acids Res.* 2014;42(22):14042-14052.

12. Spahn CM, et al. Domain movements of elongation factor eEF2 and the eukaryotic 80S ribosome facilitate tRNA translocation. *EMBO J.* 2004;23(5):1008-1019.

13. Wang C, et al. Real-time imaging of translation on single mRNA transcripts in live cells. *Cell.* 2016;165(4):990-1001.